FURTHER THEORETICAL CONSIDERATIONS OF TROPOSPHERIC WAVE MOTIONS IN EQUATORIAL LATITUDES

WALTER JAMES KOSS

National Hurricane Research Laboratory, Institute for Atmospheric Sciences, ESSA, Miami, Fla.

ABSTRACT

The known general solution of the system of linearized equations for non-viscous, adiabatic, quasi-hydrostatic flow on an equatorially oriented β-plane is examined in detail for various boundary conditions imposed on the motion. The base state is a space-time invariant zonal current. The particular solutions examined are those in which the meridional wind component is distributed either symmetrically or asymmetrically about the equator, and is constrained either to vanish at finite distance from the equator or to decay exponentially at large distance from the equator. The various solutions considered depict disturbances which are characterized by (1) very small values of divergence which increase with wavelength (in most cases), (2) relative vorticity which is meteorologically reasonable, and (3) in general, a non-geostrophic wind-pressure relationship.

1. INTRODUCTION

In a recent study, Rosenthal [1] obtained the general solution of the linearized system of equations for non-viscous, adiabatic, quasi-hydrostatic flow on an equatorially oriented β-plane. Rosenthal examined one particular solution in detail, that in which the meridional wind component was symmetric with respect to the equator and decayed exponentially with the square of the distance from the equator. Subsequently, Matsuno [2] solved a similar system of equations. He considered a class of particular solutions in which the meridional wind is constrained to approach zero as the distance from the equator approaches infinity. Rosenthal's solution was among those treated by Matsuno. Both Rosenthal and Matsuno were concerned with the extent to which their wave solutions could be considered meteorological rather than inertia-gravitational in nature. Matsuno proceeded by examining the frequency as a function of wavelength and by pictorial comparisons between wind and pressure fields for several of his cases. Rosenthal, on the other hand, made detailed studies of the wind, pressure, vorticity, and divergence fields and performed numerous calculations which clearly showed the meteorological nature of the system.

In this report, other particular solutions are examined in detail, specifically, solutions in which the meridional velocity is required to vanish at fixed distances from the equator. The format of the study is similar to that of Rosenthal.

In view of the fact that neither Matsuno's nor Rosenthal's model provides a source of perturbation energy, the solutions cannot describe the life cycles of the disturbances under consideration. The results then are artificial in the sense that waves of this type are relatively steady for all time and no information is provided concerning their origin. However, as pointed out by Rosenthal [1], they do have a remarkable similarity to the equatorial disturbances discussed by Palmer [3]. Furthermore, it would seem that an understanding of the dynamics of these simple disturbances is a mandatory prerequisite to understanding the dynamics of equatorial disturbances in the real atmosphere.

2. THE SOLUTIONS

The reader is directed to Rosenthal's paper for the complete development of the general solution which describes the model; here only a brief outline of the development will be presented. Notation is consistent with that of Rosenthal.

The linearized equations for non-viscous, adiabatic, quasi-hydrostatic, β-plane flow are

$$\frac{\partial u}{\partial t}+U\frac{\partial u}{\partial x}-\beta yv+\frac{\partial \phi}{\partial x}=0 \tag{1}$$

$$\frac{\partial v}{\partial t}+U\frac{\partial v}{\partial x}+\beta yu+\frac{\partial \phi}{\partial y}=0 \tag{2}$$

$$\frac{\partial^2 \phi}{\partial p \partial t}+U\frac{\partial^2 \phi}{\partial p \partial x}+\bar{\sigma}\omega=0 \tag{3}$$

$$\frac{\partial \omega}{\partial p}=-\left(\frac{\partial u}{\partial x}+\frac{\partial v}{\partial y}\right). \tag{4}$$

Here u, v, ω, and ϕ are, respectively, the perturbation zonal wind component, meridional wind component, p-system vertical motion, and geopotential of the isobaric surfaces; t is time, x is zonal distance, y is meridional distance measured positive northward from the equator, p is pressure, and β is the meridional rate of change of the Coriolis parameter f. Here, β=constant. $\bar{\phi}=\bar{\phi}(y,p)$, U, and

$$\bar{\sigma}=\frac{\partial^2\bar{\phi}}{\partial p^2}+\left(\frac{c_v}{c_p}\right)\frac{1}{p}\frac{\partial \phi}{\partial p} \tag{5}$$

are base state quantities with U and $\bar{\sigma}$ assumed constant.

With the condition that v be a maximum at $x=0$, $p=p_0$, and $t=0$, the system of equations (1), (2), (3), (4) has solutions of the form

$$u=A(y)\ \sin k(x-ct)\ \cos\ m(p-p_0) \tag{6}$$

$$v=B(y)\ \cos k(x-ct)\ \cos\ m(p-p_0) \tag{7}$$

$$\phi=H(y)\ \sin k(x-ct)\ \cos\ m(p-p_0) \tag{8}$$

$$\omega=W(y)\ \cos k(x-ct)\ \sin\ m(p-p_0) \tag{9}$$

where $k=2\pi/L$, L is the wavelength, c equals the wave speed, and $m=n\pi/p_0$, $n=1, 2, \ldots$. Substitution of equations (6), (7), (8), (9) into equations (1), (2), (3), (4) yields a system of linear differential equations in which the dependent variables are the coefficients $A(y)$, $B(y)$, $H(y)$, and $W(y)$. This system may be reduced to a second order differential equation for the coefficient $B=B(y)$:

$$\frac{d^2B}{dy^2}-\left(k^2-\frac{\beta}{\Delta}+\frac{\beta^2y^2}{\gamma^2}-\frac{\Delta^2k^2}{\gamma^2}\right)B=0 \tag{10}$$

where $\gamma=\bar{\sigma}^{1/2}/m$ and $\Delta=U-c$. Equation (10) transforms into a special case of the confluent hypergeometric equation which is solved to yield the following general solution for $B(y)$:

$$B=K_1e^{-\beta y^2/2\gamma}M\left(-\frac{\alpha}{2},\frac{1}{2},\frac{\beta y^2}{\gamma}\right)$$

$$+K_2y\left(\frac{\beta}{\gamma}\right)^{1/2}e^{-\beta y^2/2\gamma}M\left(\frac{1}{2}-\frac{\alpha}{2},\frac{3}{2},\frac{\beta y^2}{\gamma}\right). \tag{11}$$

Here K_1 and K_2 are arbitrary constants, $M(a, b, Z)$ is the confluent hypergeometric function [4], and

$$\alpha=\frac{\gamma[\beta-k^2\Delta(1-\Delta^2/\gamma^2)]-\Delta\beta}{2\Delta\beta}. \tag{12}$$

Values of α are determined by the side conditions imposed upon the motion. Rearrangement of the terms in equation (12) gives the frequency equation

$$\Delta^3-\frac{1}{k^2}(k^2\gamma^2+\gamma\beta+2\alpha\beta\gamma)\Delta+\frac{\gamma^2\beta}{k^2}=0 \tag{13}$$

which determines the wave speed ($c=U-\Delta$). In general, the analytic expressions for the roots of equation (13) are algebraically complicated [5] (see Appendix) and cannot be interpreted in a simple manner as was the case with Rosenthal's frequency equation.

By setting $K_2=0$, we have the solution,

$$B_1=K_1e^{-\beta y^2/2\gamma}M\left(-\frac{\alpha}{2},\frac{1}{2},\frac{\beta y^2}{\gamma}\right) \tag{14}$$

in which v is symmetric about the equator and which will be called the Symmetric Mode.

With $K_1=0$, we have,

$$B_2=K_2y\left(\frac{\beta}{\gamma}\right)^{1/2}e^{-\beta y^2/2\gamma}M\left(\frac{1}{2}-\frac{\alpha}{2},\frac{3}{2},\frac{\beta y^2}{\gamma}\right) \tag{15}$$

and v is constrained to be asymmetric about the equator. This solution will be called the Asymmetric Mode. The particular solutions examined in the following sections will be restricted to either the Symmetric or Asymmetric Mode.

Matsuno considered only those cases in which the parameter α took on integral values. For α equal to an even integer, equation (14) reduces to

$$B_1=K_1'e^{-\beta y^2/2\gamma}H_\alpha\left(\sqrt{\frac{\beta}{\gamma}}y\right), \tag{14a}$$

and for α equal to an odd integer equation (15) becomes

$$B_2=K_2'e^{-\beta y^2/2\gamma}H_\alpha\left(\sqrt{\frac{\beta}{\gamma}}y\right) \tag{15a}$$

where $H_n(x)$ is the Hermite polynomial of order n. Matsuno took the solution (14a) for even integral values of α and (15a) for odd integral values of α. These are the only solutions which do not tend toward infinity as y becomes large.

If, however, we limit the solutions to a zonal channel centered on the equator and enforce the boundary condition $v=0$ at $y=\pm y_w$ (y_w finite), then α is determined as $\alpha=\alpha^*$ where

$$M\left(-\frac{\alpha^*}{2},\frac{1}{2},\frac{\beta y_w^2}{\gamma}\right)=0 \tag{16a}$$

or

$$M\left(\frac{1}{2}-\frac{\alpha^*}{2},\frac{3}{2},\frac{\beta y_w^2}{\gamma}\right)=0 \tag{16b}$$

depending upon whether the Symmetric or Asymmetric Mode is being considered. For these solutions, the fact that B_1 and B_2 approach infinity as y approaches infinity

is irrelevant since we are concerned with only the domain $|y| \leq |y_w|$. We feel that this is a reasonable approach since we are interested in disturbances which have their maximum amplitude in low latitudes and are undetectable at higher latitudes. Also, since the approximation $f=\beta y$ becomes very poor as y becomes large, the system (1), (2), (3), (4) is unrealistic at large y. This is a second reason for restricting the solutions to a band of latitudes near the equator.

For arbitrary values of y_w, α^* must be found numerically through an iterative procedure which operates on a truncated form of $M(a, b, Z)$. Figure 1 shows values obtained in this way. As y_w becomes large, $\alpha_S \to 0$ and $\alpha_A \to 1$. As y_w becomes small, α_S and α_A both tend toward infinity.

By use of equations (1), (2), (3), (4), (6), (7), (8), (9), the remaining amplitude functions are given by

$$A(y)=\frac{\gamma^2}{k(\Delta^2-\gamma^2)}\left[\frac{dB}{dy}+\frac{\Delta\beta y}{\gamma^2}B\right] \tag{17}$$

$$H(y)=\frac{\beta y}{k}B-\Delta A \tag{18}$$

and

$$W(y)=\frac{mk\Delta}{\bar{\sigma}}H. \tag{19}$$

THE SYMMETRIC MODE

If we require that $v=v_0$ at $x=0$, $y=0$, $t=0$, we have, from equations (7) and (14),

$$B_1(0)=K_1=v_0$$

and

$$B_1=v_0 e^{-\beta y^2/2\gamma} M\left(-\frac{\alpha}{2}, \frac{1}{2}, \frac{\beta y^2}{\gamma}\right). \tag{20}$$

Substitution of equation (20) into equations (17), (18), and (19) yields the Symmetric Mode solutions for the perturbation quantities u, v, ϕ, and ω.

$$u=\frac{v_0\beta y}{k(\Delta+\gamma)} e^{-\beta y^2/2\gamma}\left\{M-\frac{2\alpha\gamma}{\Delta-\gamma}M^*\right\} \times \sin k(x-ct) \cos m(p-p_0) \tag{21}$$

$$v=v_0 e^{-\beta y^2/2\gamma} M \cos k(x-ct) \cos m(p-p_0) \tag{22}$$

$$\phi=\frac{v_0\gamma\beta y}{k(\Delta+\gamma)} e^{-\beta y^2/2\gamma}\left\{M+\frac{2\alpha\Delta}{\Delta-\gamma}M^*\right\} \times \sin k(x-ct) \cos m(p-p_0) \tag{23}$$

and

$$\omega=\frac{v_0\Delta\beta y}{\bar{\sigma}^{1/2}(\Delta+\gamma)} e^{-\beta y^2/2\gamma}\left\{M+\frac{2\alpha\Delta}{\Delta-\gamma}M^*\right\} \times \cos k(x-ct) \sin m(p-p_0) \tag{24}$$

where

$$M=M\left(-\frac{\alpha}{2}, \frac{1}{2}, \frac{\beta y^2}{\gamma}\right) \tag{24a}$$

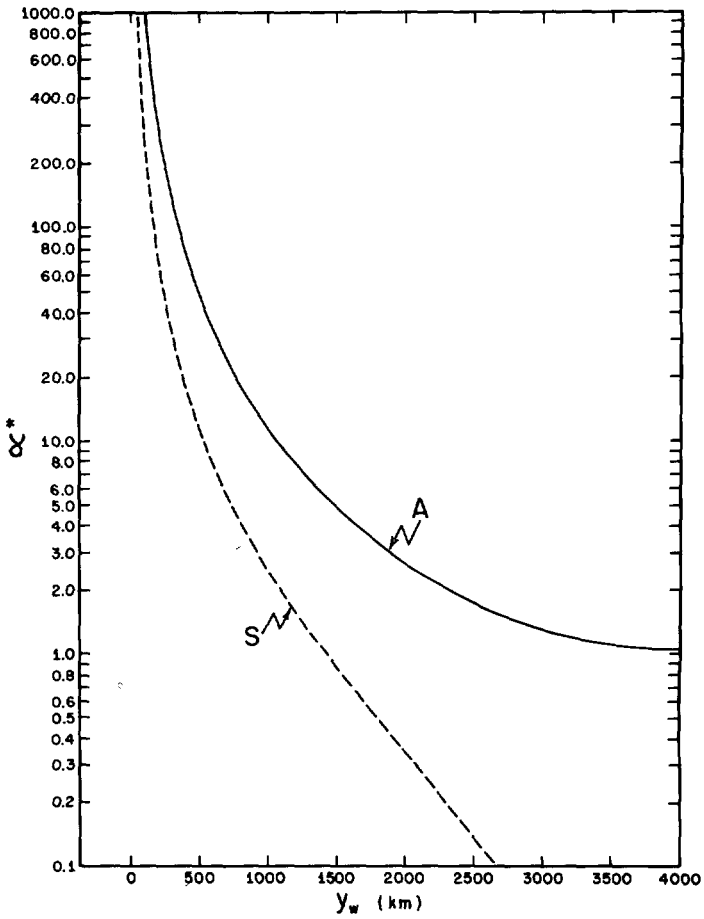

FIGURE 1.—Values of α^* and y_w such that equations (16a) and (16b) are satisfied. S and A denote, respectively, the curves which give values of α^* appropriate for the Symmetric and Asymmetric Modes.

and

$$M^*=M\left(1-\frac{\alpha}{2}, \frac{3}{2}, \frac{\beta y^2}{\gamma}\right). \tag{24b}$$

From (22),

$$v_{max} \equiv v_0$$

for all cases in the Symmetric Mode.

By setting $\alpha=0$,

$$B_1=v_0 e^{-\beta y^2/2\gamma} \tag{25}$$

since

$$M\left(0, \frac{1}{2}, \frac{\beta y^2}{\gamma}\right) \equiv 1;$$

this is the case treated by Rosenthal [1].

In this case the solutions for u, v, ϕ, and ω reduce to

$$u=\frac{v_0\beta y}{k(\Delta+\gamma)} e^{-\beta y^2/2\gamma} \sin k(x-ct) \cos m(p-p_0) \tag{26}$$

$$v=v_0 e^{-\beta y^2/2\gamma} \cos k(x-ct) \cos m(p-p_0) \tag{27}$$

$$\phi=\frac{v_0\gamma\beta y}{k(\Delta+\gamma)}\,e^{-\beta y^2/2\gamma}\sin k(x-ct)\cos m(p-p_0) \quad (28)$$

and

$$\omega=\frac{v_0\Delta\beta y}{\sigma^{1/2}(\Delta+\gamma)}\,e^{-\beta y^2/2\gamma}\cos k(x-ct)\sin m(p-p_0). \quad (29)$$

THE ASYMMETRIC MODE

Substitution of equation (15) into equations (17), (18), and (19) gives the amplitudes of the perturbation quantities for the Asymmetric Mode. The solutions for u, v, ϕ, and ω are

$$u=\frac{K_2\left(\frac{\beta}{\gamma}\right)^{1/2}}{k(\Delta^2-\gamma^2)}\,e^{-\beta y^2/2\gamma}\left\{\frac{2}{3}(1-\alpha)\gamma\beta y^2\tilde{M}^*+[\gamma^2+(\Delta-\gamma)\beta y^2]\tilde{M}\right\}\sin k(x-ct)\cos m(p-p_0) \quad (30)$$

$$v=K_2 y\left(\frac{\beta}{\gamma}\right)^{1/2}e^{-\beta y^2/2\gamma}\tilde{M}\cos k(x-ct)\cos m(p-p_0) \quad (31)$$

$$\phi=\frac{K_2(\beta\gamma)^{1/2}}{k(\Delta^2-\gamma^2)}\,e^{-\beta y^2/2\gamma}\left\{\frac{2}{3}(\alpha-1)\Delta\beta y^2\tilde{M}^*+[(\Delta-\gamma)\beta y^2-\Delta\gamma]\tilde{M}\right\}\sin k(x-ct)\cos m(p-p_0) \quad (32)$$

and

$$\omega=K_2\left(\frac{\beta}{\sigma\gamma}\right)^{1/2}\frac{\Delta}{\Delta^2-\gamma^2}\,e^{-\beta y^2/2\gamma}\left\{\frac{2}{3}(\alpha-1)\Delta\beta y^2\tilde{M}^*+[(\Delta-\gamma)\beta y^2-\Delta\gamma]\tilde{M}\right\}\cos k(x-ct)\sin m(p-p_0) \quad (33)$$

where

$$\tilde{M}=M\left(\frac{1}{2}-\frac{\alpha}{2},\frac{3}{2},\frac{\beta y^2}{\gamma}\right) \quad (33a)$$

and

$$\tilde{M}^*=M\left(\frac{3}{2}-\frac{\alpha}{2},\frac{5}{2},\frac{\beta y^2}{\gamma}\right). \quad (33b)$$

The asymmetric case analogous to (25) is obtained by setting $\alpha=1$. This gives

$$B_2=K_2 y\left(\frac{\beta}{\gamma}\right)^{1/2}e^{-\beta y^2/2\gamma}. \quad (34)$$

For the Asymmetric Decay case,[1] the solutions for u, v, ϕ, and ω are

$$u=\frac{K_2[\gamma^2+(\Delta-\gamma)\beta y^2]}{k(\Delta^2-\gamma^2)}\left(\frac{\beta}{\gamma}\right)^{1/2}e^{-\beta y^2/2\gamma}\times\{\sin k(x-ct)\cos m(p-p_0)\} \quad (35)$$

$$v=K_2 y\left(\frac{\beta}{\gamma}\right)^{1/2}e^{-\beta y^2/2\gamma}\cos k(x-ct)\cos m(p-p_0) \quad (36)$$

$$\phi=\frac{K_2[(\Delta-\gamma)\beta y^2-\Delta\gamma]}{k(\Delta^2-\gamma^2)}(\beta\gamma)^{1/2}e^{-\beta y^2/2\gamma}\times\{\sin k(x-ct)\cos m(p-p_0)\} \quad (37)$$

and

$$\omega=\frac{K_2[(\Delta-\gamma)\beta y^2-\Delta\gamma]}{(\Delta^2-\gamma^2)}\Delta\left(\frac{\beta}{\sigma\gamma}\right)^{1/2}e^{-\beta y^2/2\gamma}\times\{\cos k(x-ct)\sin m(p-p_0)\}. \quad (38)$$

In the Asymmetric Mode, $|v|$ is a maximum (v_{max}) at $y=y_m$ where y_m satisfies the condition

$$\left(1-\frac{\beta y_m^2}{\gamma}\right)\tilde{M}_{y=y_m}+\frac{2}{3}(1-\alpha)\frac{\beta y_m^2}{\gamma}\tilde{M}^*_{y=y_m}=0 \quad (39)$$

and

$$K_2=\frac{v_{max}}{\left[\left(\frac{\beta}{\gamma}\right)^{1/2}y_m e^{-\frac{\beta y_m^2}{2\gamma}}\tilde{M}_{y=y_m}\right]}. \quad (40)$$

3. DISCUSSION

Table 1 lists the three roots of the frequency equation (13). Table 1c lists values of the roots compared with

$$\Delta_{ND}=\frac{\beta}{k^2+\epsilon(\pi/y_w)^2}$$

which is the value of Δ appropriate for nondivergent motion. The parameter ϵ is ¼ in the Symmetric Mode, 1 in the Asymmetric Mode, and zero in the decay cases for both modes. For the wavelengths considered, the roots Δ_1 and Δ_2 correspond to rapidly moving inertia-gravity waves. The meteorologically significant root, which gives small phase speeds relative to the basic current for wavelengths in the synoptic range, is Δ_3. As pointed out by Matsuno [2], Δ_3 can become quite large at very long wavelengths. However, the wavelengths at which this occurs are far larger than those considered here and, in fact, are probably large enough to invalidate the β-plane approximation.

Further discussion will be limited to the root Δ_3 and the subscript will be omitted. Comparison of Δ with Δ_{ND} shows that in both modes the difference $\Delta_{ND}-\Delta$ increases

[1] For reference purposes, solutions (25) and (34) will be referred to, respectively, as the "Symmetric Decay case" and the "Asymmetric Decay case."

TABLE 1.—*Values of* Δ_1, Δ_2, Δ_3, Δ_{ND}, $\Delta_{ND}-\Delta_3$, *computed from the frequency equation.* Δ_{ND} *is a value of* Δ *appropriate for nondivergent motion. Units are m./sec., n corresponds to the number of levels of nondivergence, and* $\bar{\sigma}=3$ *m.t.s. units*

L(km.)	$n=1$						$n=2$					
	Symmetric			Asymmetric			Symmetric			Asymmetric		
	Decay	$\lvert y_w\rvert=$ 2375 km.	$\lvert y_w\rvert=$ 1125 km.	Decay	$\lvert y_w\rvert=$ 2375 km.	$\lvert y_w\rvert=$ 1125 km.	Decay	$\lvert y_w\rvert=$ 2375 km.	$\lvert y_w\rvert=$ 1125 km.	Decay	$\lvert y_w\rvert=$ 2375 km.	$\lvert y_w\rvert=$ 1125 km.
(a) Values of Δ_1												
1000	−55.7	−55.8	−56.8	−56.3	−56.8	−60.6	−28.1	−28.1	−28.5	−28.7	−28.8	−30.5
2000	−57.4	−57.7	−61.3	−59.5	−61.4	−74.5	−29.7	−29.8	−31.2	−31.7	−32.0	−37.8
3000	−59.9	−60.1	−68.1	−64.4	−68.3	−93.0	−32.0	−32.1	−35.1	−36.1	−36.7	−47.3
4000	−63.2	−64.5	−76.5	−70.5	−76.8	−113.9	−34.9	−35.0	−40.0	−41.2	−42.1	−58.0
5000	−67.0	−68.9	−85.8	−77.5	−86.2	−136.0	−38.1	−38.2	−44.7	−46.8	−48.1	−69.2
(b) Values of Δ_2												
1000	55.1	55.2	56.2	55.7	56.2	60.1	27.6	27.6	28.0	28.1	28.2	30.0
2000	55.1	55.5	59.4	57.4	59.5	73.2	27.6	27.6	29.3	29.9	30.2	36.5
3000	55.1	56.1	64.5	60.3	64.8	91.2	27.6	27.7	31.5	32.7	33.5	45.5
4000	55.1	56.8	71.2	64.3	71.6	111.7	27.6	27.8	34.5	36.5	37.7	55.8
5000	55.1	57.9	79.3	69.3	79.8	133.6	27.6	28.0	38.2	41.1	42.8	66.8
(c) Values of Δ_3, Δ_{ND}, $\Delta_{ND}-\Delta_3$												
1000 Δ_{ND}	0.579	0.573	0.552	0.579	0.555	0.484	0.579	0.573	0.552	0.579	0.555	0.484
1000 Δ_3	0.573	0.571	0.552	0.562	0.551	0.483	0.567	0.567	0.551	0.545	0.542	0.481
1000 $\Delta_{ND}-\Delta_3$	0.006	0.002	0.000	0.017	0.004	0.001	0.012	0.006	0.001	0.034	0.013	0.003
2000 Δ_{ND}	2.32	2.22	1.935	2.32	1.97	1.294	2.32	2.22	1.94	2.32	1.97	1.29
2000 Δ_3	2.23	2.20	1.932	2.06	1.93	1.290	2.15	2.14	1.92	1.86	1.82	1.28
2000 $\Delta_{ND}-\Delta_3$	0.09	0.02	0.003	0.26	0.04	0.004	0.17	0.08	0.02	0.46	0.15	0.01
3000 Δ_{ND}	5.21	4.74	3.609	5.21	3.73	1.877	5.21	4.74	3.61	5.21	3.73	1.88
3000 Δ_3	4.80	4.65	3.603	4.08	3.58	1.868	4.48	4.45	3.59	3.36	3.23	1.84
3000 $\Delta_{ND}-\Delta_3$	0.41	0.09	0.006	1.13	0.15	0.009	0.73	0.29	0.02	1.85	0.50	0.04
4000 Δ_{ND}	9.27	7.87	5.177	9.27	5.42	2.227	9.27	7.87	5.18	9.27	5.42	2.23
4000 Δ_3	8.08	7.68	5.169	6.21	5.12	2.215	7.32	7.23	5.15	4.68	4.43	2.18
4000 $\Delta_{ND}-\Delta_3$	1.19	0.19	0.008	3.06	0.30	0.012	1.95	0.64	0.03	4.59	0.99	0.05
5000 Δ_{ND}	14.48	11.34	6.480	14.48	6.87	2.438	14.48	11.34	6.48	14.48	6.87	2.44
5000 Δ_3	11.91	11.02	6.468	8.20	6.39	2.423	10.49	10.29	6.43	5.72	5.35	2.38
5000 $\Delta_{ND}-\Delta_3$	2.57	0.32	0.012	6.28	0.48	0.015	3.99	1.05	0.05	8.76	1.52	0.06

with wavelength and y_w. This implies that the model divergence has greater significance at longer wavelengths, but for a given wavelength the significance diminishes as the latitudinal extent of the perturbation is reduced. In general, the model divergence appears to be more significant in the Asymmetric Mode.

As was pointed out by Rosenthal for the Symmetric Decay case, the effect of the divergence is a retardation of the westward movement of the perturbations relative to the basic current as is evidenced by the difference $\Delta_{ND}-\Delta$. Hence, in both modes, the divergence patterns must be as described by Rosenthal; i.e., there is divergence to the west of the cyclonic relative vorticity centers and convergence to the east of these centers.[2] Also, we can expect the magnitude of the Asymmetric Mode divergences to be larger than those of the Symmetric Mode.

The amplitudes of the model relative vorticity $\hat{\zeta}$ and the model divergence $\hat{D}$ can be written in terms of the amplitude of v,

$$\hat{\zeta}=-kB-\frac{\gamma^2}{k(\Delta^2-\gamma^2)}\left\{\left[k^2-\frac{\beta}{\Delta}+\frac{1}{\gamma^2}(\beta^2y^2-\Delta^2k^2)\right]B+\frac{\Delta\beta}{\gamma^2}\left(B+y\frac{dB}{dy}\right)\right\}, \quad (41)$$

and

$$\hat{D}=\frac{\Delta}{\Delta^2-\gamma^2}\left[\Delta\frac{dB}{dy}+\beta yB\right]. \quad (42)$$

In the Symmetric Mode, $|\hat{\zeta}|$ is a maximum at the equator,

$$|\hat{\zeta}|_{max}=\left|\frac{\beta v_0}{\Delta k}\right| \quad (43)$$

which is a function of wavelength and y_w (through Δ).[3] Table 2 lists values of $|\hat{\zeta}|_{max}$ for this mode. In the Asymmetric Mode, $\hat{\zeta}=0$ at the equator and maximum values of $|\hat{\zeta}|$ occur at points symmetrically equidistant from the equator. Table 3 lists values of $|\hat{\zeta}|_{max}$ along with the distances from the equator at which they occur.

Both tables 2 and 3 show that $|\hat{\zeta}|_{max}$ has a magnitude which is meteorologically significant and which decreases with increasing wavelength except in the cases $y_w=\pm1125$

[2] This follows from an examination of the model vorticity equation

$$\frac{D}{Dt}\left(\frac{\partial v}{\partial x}-\frac{\partial u}{\partial y}\right)=-\beta y\left(\frac{\partial u}{\partial x}+\frac{\partial v}{\partial y}\right)-\beta v.$$

[3] Rosenthal's equation (51) reduces to (43).

TABLE 2.—*Values of* $\hat{\zeta}_{max}$ *for the cases in the Symmetric Mode.* $v_0=5$ *m.p.s.,* $\bar{\sigma}=3$ *m.t.s. Values are scaled by* 10^5 *and are in units of sec.*$^{-1}$

L (km.)	$n=1$			$n=2$		
	Decay	$y_w=\pm 2375$ km.	$y_w=\pm 1125$ km.	Decay	$y_w=\pm 2375$ km.	$y_w=\pm 1125$ km.
1000	3.17	3.19	3.30	3.21	3.21	3.30
2000	1.63	1.66	1.88	1.69	1.70	1.89
3000	1.14	1.17	1.51	1.22	1.23	1.52
4000	0.90	0.95	1.41	0.99	1.01	1.41
5000	0.76	0.82	1.41	0.87	0.88	1.41

TABLE 3.—*Values of* $|\hat{\zeta}|_{max}$ *for the cases in the Asymmetric Mode.* $v_{max}=5$ *m.p.s.,* $\bar{\sigma}=3$ *m.t.s. Values are scaled by* 10^5 *and are in units of sec.*$^{-1}$ δ *is the approximate distance (in km.) from the equator of the maximum values*

Case	L (km.)	$n=1$		$n=2$	
		$\lvert\hat{\zeta}\rvert_{max}\times 10^5$	δ	$\lvert\hat{\zeta}\rvert_{max}\times 10^5$	δ
Decay	1000	3.21	1550	3.27	1125
	2000	1.70	1500	1.83	1050
	3000	1.24	1450	1.44	1000
	4000	1.05	1400	1.31	950
	5000	0.96	1375	1.29	925
$y_w=\pm 2375$ km	1000	3.25	1150	3.30	1025
	2000	1.84	1125	1.89	975
	3000	1.46	1100	1.53	930
	4000	1.34	1090	1.43	915
	5000	1.32	1085	1.43	910
$y_w=\pm 1125$ km	1000	3.75	560	3.76	550
	2000	2.82	560	2.83	550
	3000	2.91	560	2.92	550
	4000	3.27	560	3.28	550
	5000	3.73	560	3.74	550

km. For this y_w, in the Symmetric Mode, $|\hat{\zeta}|_{max}$ has minimum values for wavelengths in the 4000–5000-km. range although this is not clear from the table. In the Asymmetric Mode, minimum values of $|\hat{\zeta}|_{max}$ occur for wavelengths in the 2000–3000-km. range.

Maximum values of $|\hat{D}|$ are found at points symmetrically equidistant from the equator in both modes. Tables 4 and 5 list values of $|\hat{D}|_{max}$ along with the approximate distance of the maxima from the equator. In the Symmetric Mode this distance is given by $y=y_m$ which satisfies the condition

$$[k^2\Delta(\gamma^2-\Delta^2)+\beta^2y_m^2(\Delta-\gamma)]\tilde{M}_{y=y_m}-2\alpha\Delta\beta^2y_m^2\tilde{M}^*_{y=y_m}=0. \quad (44)$$

For the decay case,

$$y_m=\pm\left(\frac{\gamma}{\beta}\right)^{1/2}. \quad (45)$$

Maximum values of $|\hat{D}|$ are then given by[4] (in the decay case)

$$|\hat{D}_S|_{max}=\left|\frac{\Delta v_0}{(\Delta+\gamma)}\left(\frac{\beta}{\gamma e}\right)^{1/2}\right|. \quad (46)$$

[4] Equations (45) and (46) are identical to Rosenthal's equations (50).

TABLE 4.—*Values of* $|\hat{D}|_{max}$ *for the cases in the Symmetric Mode.* $v_{max}=5$ *m.p.s.,* $\bar{\sigma}=3$ *m.t.s. Values are scaled by* 10^7 *and are in units of sec.*$^{-1}$. δ *is the approximate distance (in kilometers) from the equator of the maximum values.*

Case	L (km.)	$n=1$		$n=2$	
		$\lvert\hat{D}\rvert_{max}\times 10^7$	δ	$\lvert\hat{D}\rvert_{max}\times 10^7$	δ
Decay	1000	0.20	$\sqrt{\frac{\gamma}{\beta}}\sim 1560$	0.56	$\sqrt{\frac{\gamma}{\beta}}\sim 1100$
	2000	0.76		2.00	
	3000	1.56		3.86	
	4000	2.50		5.80	
	5000	3.47		7.62	
$y_w=\pm 2375$ km	1000	0.17	1260	0.54	1055
	2000	0.61	1225	1.93	1045
	3000	1.19	1200	3.68	1040
	4000	1.79	1175	5.43	1035
	5000	2.31	1160	6.95	1030
$y_w=\pm 1125$ km	1000	0.08	605	0.31	600
	2000	0.23	575	0.90	565
	3000	0.33	540	1.30	525
	4000	0.35	500	1.38	475
	5000	0.32	440	1.25	425

TABLE 5.—*Values of* $|\hat{D}|_{max}$ *for the cases in the Asymmetric Mode. Same remarks as table 4*

Case	L (km.)	$n=1$		$n=2$	
		$\lvert\hat{D}\rvert_{max}\times 10^7$	δ	$\lvert\hat{D}\rvert_{max}\times 10^7$	δ
Decay	1000	0.40	2190	1.08	1560
	2000	1.43	2175	3.62	1540
	3000	2.80	2150	6.43	1505
	4000	4.22	2125	8.90	1465
	5000	5.52	2090	10.90	1425
$y_w=\pm 2375$ km	1000	0.27	1490	0.98	1375
	2000	0.93	1460	3.22	1350
	3000	1.67	1435	5.62	1325
	4000	2.35	1400	7.57	1300
	5000	2.89	1365	9.05	1275
$y_w=\pm 1125$ km	1000	0.11	700	0.45	700
	2000	0.29	675	1.14	670
	3000	0.40	650	1.59	630
	4000	0.47	625	1.86	615
	5000	0.51	590	2.01	585

In the Asymmetric Mode, the distances from the equator to the divergence maxima are given by $y=y_m$ which satisfy the condition

$$[\Delta k^2(\gamma^2-\Delta^2)+\beta^2y_m^2(\Delta-\gamma)+\beta\gamma^2]\tilde{M}_{y=y_m}+\frac{2}{3}(1-\alpha)\gamma\beta^2y_m^2\tilde{M}^*_{y=y_m}=0. \quad (47)$$

In the decay case,

$$y_m=\pm\left[\frac{\gamma}{\beta}\left(\frac{3\Delta-2\gamma}{\Delta-\gamma}\right)\right]^{1/2}, \quad (48)$$

and

$$|\hat{D}_A|_{max}=\left|2v_{max}\left(\frac{\Delta}{\Delta+\gamma}\right)\left(\frac{\beta}{\gamma}\right)^{1/2}e^{-\frac{1}{2}\left(\frac{2\Delta-\gamma}{\Delta-\gamma}\right)}\right|. \quad (49)$$

Analysis of the ratio $|\hat{D}_A|_{max}/|\hat{D}_S|_{max}$ (equations (46) and (49)) shows that in the decay case the Asymmetric Mode divergences are larger than those of the Symmetric Mode for all wavelengths under consideration. The values of

TABLE 6.—*Values of the ratio* $\left|\frac{f\nabla\cdot\mathbf{V}}{\beta v}\right|$

Lat. (deg.)	$L=2000$, $n=1$			$L=5000$, $n=2$		
	Decay	$\lvert y_w\rvert=2375$ km.	$\lvert y_w\rvert=1125$ km.	Decay	$\lvert y_w\rvert=2375$ km.	$\lvert y_w\rvert=1125$ km.
	Symmetric Mode					
20.0	0.08	0.06	----------	1.11	0.75	----------
17.5	0.06	0.05	----------	0.85	0.53	----------
15.0	0.04	0.04	----------	0.62	0.53	----------
12.5	0.03	0.03	----------	0.43	0.39	----------
10.0	0.02	0.02	∞*	0.29	0.27	∞*
7.5	0.01	0.01	0.007	0.16	0.15	0.027
5.0	0.005	0.005	0.003	0.07	0.07	0.017
2.5	0.001	0.001	0.001	0.02	0.02	0.007
0	0.0	0.0	0.0	0.0	0.0	0.0
	Asymmetric Mode					
20.0	0.07	0.05	----------	0.74	0.25	----------
17.5	0.06	0.05	----------	0.57	0.45	----------
15.0	0.04	0.04	----------	0.44	0.37	----------
12.5	0.03	0.03	----------	0.32	0.28	----------
10.0	0.02	0.02	∞*	0.22	0.20	∞*
7.5	0.01	0.01	0.006	0.14	0.13	0.032
5.0	0.006	0.006	0.003	0.09	0.08	0.022
2.5	0.002	0.002	0.001	0.06	0.05	0.012

*The ratio is infinite at 1125 km.

TABLE 7.—*Values of the ratio* $|\hat{D}|_{max}/|\hat{\zeta}|_{max}$

Case	L (km)	Symmetric	Asymmetric
(a) $n=1$			
Decay	1000	6.34×10^{-4}	1.23×10^{-3}
	2000	4.66×10^{-3}	8.41×10^{-3}
	3000	1.37×10^{-2}	2.26×10^{-2}
	4000	2.78×10^{-2}	4.02×10^{-2}
	5000	4.57×10^{-2}	5.75×10^{-2}
$y_w=\pm2375$ km.	1000	5.17×10^{-4}	8.31×10^{-4}
	2000	3.64×10^{-3}	5.03×10^{-3}
	3000	1.02×10^{-2}	1.14×10^{-2}
	4000	1.88×10^{-2}	1.75×10^{-2}
	5000	2.82×10^{-2}	2.19×10^{-2}
$y_w=\pm1125$ km.	1000	2.43×10^{-4}	3.04×10^{-4}
	2000	1.21×10^{-3}	1.03×10^{-3}
	3000	2.17×10^{-3}	1.38×10^{-3}
	4000	2.47×10^{-3}	1.44×10^{-3}
	5000	2.27×10^{-3}	1.38×10^{-3}
(b) $n=2$			
Decay	1000	1.74×10^{-3}	3.30×10^{-3}
	2000	1.18×10^{-2}	1.98×10^{-2}
	3000	3.16×10^{-2}	4.47×10^{-2}
	4000	5.86×10^{-2}	6.79×10^{-2}
	5000	8.76×10^{-2}	8.45×10^{-2}
$y_w=\pm2375$ km.	1000	1.69×10^{-3}	2.96×10^{-3}
	2000	1.14×10^{-2}	1.70×10^{-2}
	3000	2.99×10^{-2}	3.67×10^{-2}
	4000	5.38×10^{-2}	5.29×10^{-2}
	5000	7.90×10^{-2}	6.33×10^{-2}
$y_w=\pm1125$ km.	1000	9.30×10^{-4}	1.20×10^{-3}
	2000	4.75×10^{-3}	4.03×10^{-3}
	3000	8.55×10^{-3}	5.45×10^{-3}
	4000	9.79×10^{-3}	5.67×10^{-3}
	5000	8.87×10^{-3}	5.37×10^{-3}

Δ listed in table 1c suggest that this relationship holds in the other cases also.

The maximum divergences increase with wavelength except for the Symmetric Mode case with $y_w=\pm1125$ km. For this case, the divergence has maximum values for wavelengths in the 3000–4000-km. range.

The contribution of the model divergence to vorticity changes is essentially the same as that described by Rosenthal [1]. The Asymmetric Mode differs little from the Symmetric Mode. Table 6 lists values of $|f\nabla\cdot\mathbf{V}/\beta v|$ for the various cases with $L=2000$ km., $n=1$, and $L=5000$ km., $n=2$. The contribution is negligible except for the longer wavelengths with $n=2$. Here the ratio is still small when $|y_w|$ is small. However, in the decay cases and for large values of $|y_w|$, the contribution is appreciable to within 5° of the equator.

The model divergences are extremely small in comparison to the observed magnitudes associated with equatorial disturbances as given by Palmer [3]. As pointed out by Rosenthal [1], this discrepancy is probably due to the lack of a convective heat source in the model.

Values of the ratio $|\hat{D}|_{max}/|\hat{\zeta}|_{max}$ are given by table 7. We note that the ratio increases with increasing $|y_w|$. The ratio also increases with wavelength except in the cases $y_w=\pm1125$ km. Here, maximum values are found for wavelengths in the 3000–4000-km. range.

In order to examine the extent to which the perturbation flow is in geostrophic equilibrium, we define

$$R_{0x}=\left|\frac{\frac{\partial u}{\partial t}+U\frac{\partial u}{\partial x}}{\beta y v}\right| \tag{50a}$$

TABLE 8.—*Behavior of the ratios* R_{0x}, R_{0y} *at the equator and at the meridional extreme of their definition*

	Evaluated at $y=0$	Evaluated at $y=\pm y_w$	$\lim y\to\infty$
R^S_{0x}	$\left\lvert\frac{\Delta[(\Delta-\gamma)-2\alpha\gamma]}{\Delta^2-\gamma^2}\right\rvert$	∞	
R^{SD}_{0x}	$\left\lvert\frac{\Delta}{\Delta+\gamma}\right\rvert$		$\left\lvert\frac{\Delta}{\Delta+\gamma}\right\rvert$
R^A_{0x}	∞	∞	
R^{AD}_{0x}	∞		$\left\lvert\frac{\Delta}{\Delta+\gamma}\right\rvert$
R^S_{0y}	∞	0	
R^{SD}_{0y}	∞		0
R^A_{0y}	$\left\lvert\frac{\Delta(1+2\alpha)-\gamma}{\gamma}\right\rvert$	0	
R^{AD}_{0y}	$\left\lvert\frac{3\Delta-\gamma}{\gamma}\right\rvert$		0

and

$$R_{0y}=\left|\frac{\frac{\partial v}{\partial t}+U\frac{\partial v}{\partial x}}{\beta y u}\right|. \tag{50b}$$

Substitution of the solutions for u and v into these expressions yields

$$R^S_{0x}=\left|\frac{\Delta[(\Delta-\gamma)M-2\alpha\gamma M^*]}{(\Delta^2-\gamma^2)M}\right| \quad (51)$$

$$R^S_{0y}=\left|\frac{\Delta k^2(\Delta^2-\gamma^2)M}{\beta^2y^2[(\Delta-\gamma)M-2\alpha\gamma M^*]}\right| \quad (52)$$

$$R^A_{0x}=\left|\frac{\Delta\{\frac{2}{3}(1-\alpha)\gamma\beta y^2\tilde{M}^*+[\gamma^2+(\Delta-\gamma)\beta y^2]\tilde{M}\}}{(\Delta^2-\gamma^2)\beta y^2\tilde{M}}\right| \quad (53)$$

$$R^A_{0y}=\left|\frac{\Delta k^2(\Delta^2-\gamma^2)\tilde{M}}{\beta\{\frac{2}{3}(1-\alpha)\gamma\beta y^2\tilde{M}^*+[\gamma^2+(\Delta-\gamma)\beta y^2]\tilde{M}\}}\right| \quad (54)$$

where the superscript S refers to the Symmetric Mode and A refers to the Asymmetric Mode. (M, M^*, $\tilde{M}$, $\tilde{M}^*$ are defined by equations (24a), (24b), (33a), and (33b).) R_{0x} and R_{0y} are measures of the geostrophic equilibrium of the meridional and zonal velocity components, respectively. Small values of these ratios correspond to quasi-geostrophic motion and large values indicate highly ageostrophic flow. In the decay cases, equations (51), (52), (53), (54) reduce to the following (superscript D denotes these cases):

$$R^{SD}_{0x}=\left|\frac{\Delta}{\Delta+\gamma}\right| \quad (55)$$

$$R^{SD}_{0y}=\left|\frac{\gamma}{\beta y^2}\right| \quad (56)$$

$$R^{AD}_{0x}=\left|\frac{\Delta}{\Delta+\gamma}+\frac{\Delta\gamma^2}{(\Delta^2-\gamma^2)\beta y^2}\right| \quad (57)$$

$$R^{AD}_{0y}=\left|\frac{\gamma(3\Delta-\gamma)}{\gamma^2+(\Delta-\gamma)\beta y^2}\right|. \quad (58)$$

Table 8 summarizes the behavior of these ratios at the equator and at the latitudinal limit of their definition. The latitudinal variation of R_{0x} is shown in figure 2 for $L=2000$ km., $n=1$. For each value of y_w, R_{0x} increases with wavelength but the shapes of the curves are similar to those shown by figure 2. Except in the decay case, where R^{SD}_{0x} is independent of latitude, R^S_{0x} is smallest near the equator and approaches infinity as y approaches y_w.

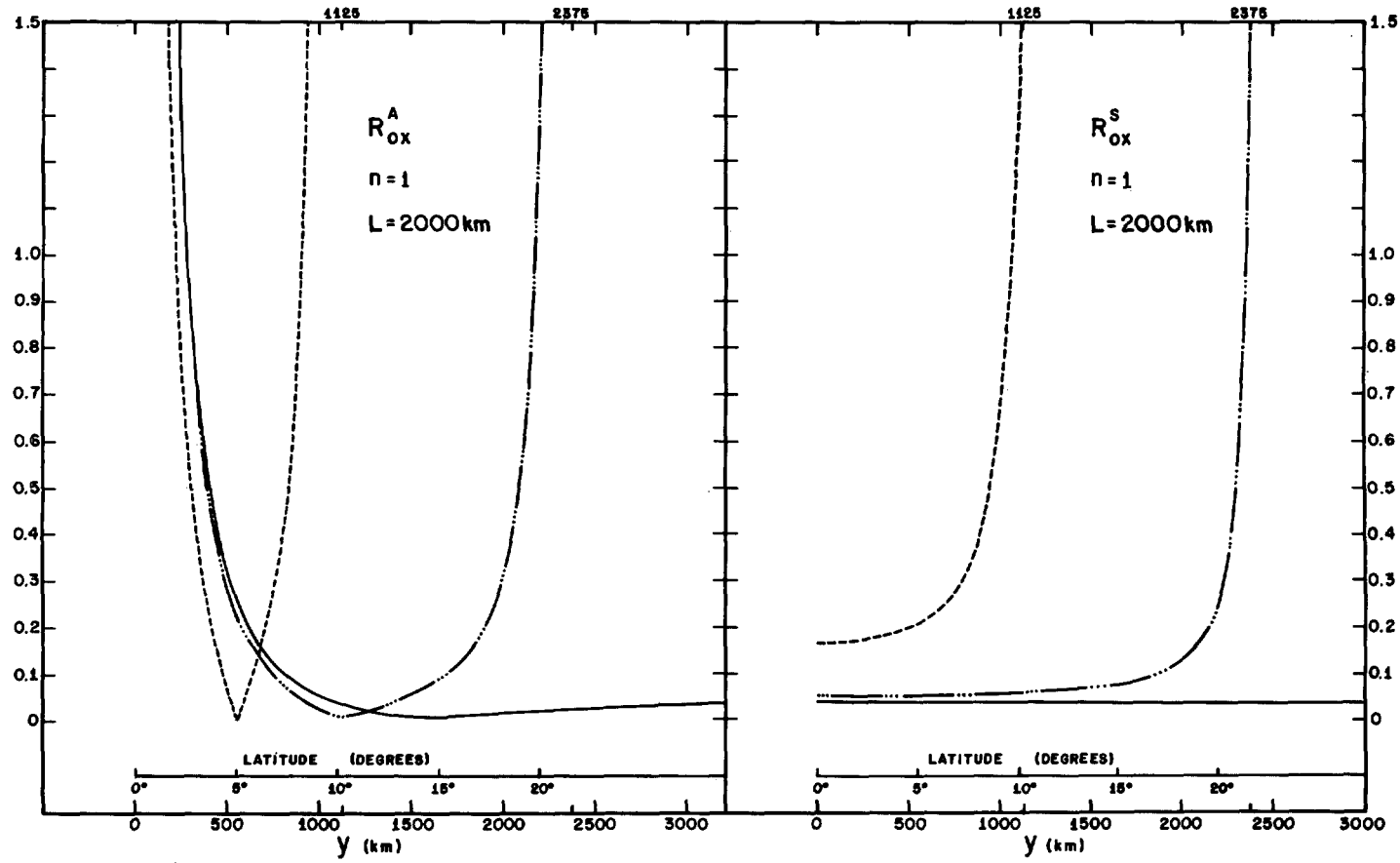

FIGURE 2.—Values of the ratio R_{0x} (equation (50a)) for cases in the Asymmetric Mode (denoted by superscript A) and Symmetric Mode (superscript S). The solid line represents values for the decay case, the broken line the case $y_w=\pm 2375$ km., and the dashed line the case $y_w=\pm 1125$ km.

Hence, in the symmetrical cases, the meridional component of the perturbation wind is most nearly geostrophic at the equator and becomes increasingly ageostrophic at higher latitudes. On the other hand, the perturbation v-component becomes increasingly ageostrophic in the symmetric case as the perturbations are confined to smaller and smaller (decreasing $|y_w|$) bands of latitude surrounding the equator. As indicated above, the meridional component of the perturbation wind becomes increasingly ageostrophic as the wavelength increases.

In the asymmetric cases, R^A_{0x} approaches infinity as the equator is approached. Hence, near the equator, in the Asymmetric Mode, the v-component of the perturbation wind is highly ageostrophic. In the decay case, the v-component becomes near geostrophic at higher latitudes. In the other cases, v is highly ageostrophic near $y=y_w$ as well as near the equator. Geostrophy is, however, approached in a narrow band of latitudes intermediate to the equator and $y=y_w$.

Figure 3 shows the latitudinal variation of R_{0y} for $L=2000$ km. and $n=1$. R^{SD}_{0y} is independent of wavelength. For the other cases, in contrast to R_{0x}, R_{0y} shows a small decrease with increases in wavelength. The curves for other wavelengths, however, are very much like those shown by figure 3. The values of R^S_{0y} show that the perturbation u-component is highly ageostrophic near the equator, that it becomes less ageostrophic as the meridional extent of the perturbation is diminished, and slightly less ageostrophic as the wavelength is increased.

The behavior of the u-component, in the Asymmetric Mode, is similar except that R^A_{0y} tends to infinite values near $y=1700$ km. (15° lat.) in the decay case and near $y=y_w/2$ in the other cases. As the equator is approached, the perturbation zonal wind tends toward geostrophy but R^A_{0y} still remains greater than 0.5.

Finally, we note that, in the Symmetric Mode, R_{0x} increases and R_{0y} decreases as n (the number of levels of nondivergence) increases. The opposite is true in the Asymmetric Mode. The changes in R_{0x} and R_{0y} with n are most marked when $|y_w|$ is large.

4. SYNOPTIC ASPECTS OF THE SOLUTIONS

Figures 4, 5, and 6 present analyses of the pressure and wind fields for the Asymmetric Decay case (fig. 4), the Symmetric (fig. 5) and Asymmetric (fig. 6) cases

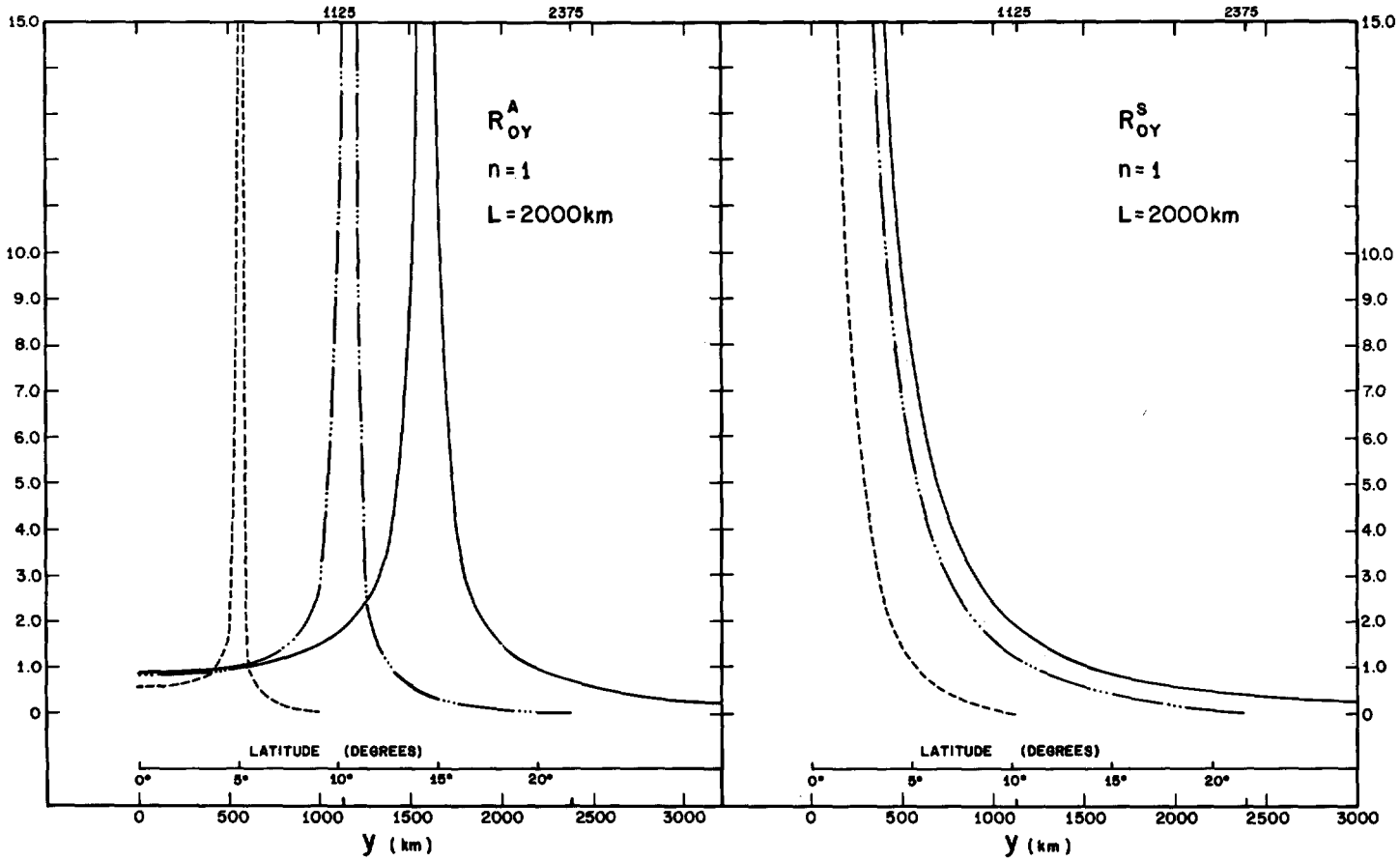

FIGURE 3.—Values of the ratio R_{0y} (equation (50b)) for cases in the Asymmetric Mode (denoted by superscript A) and Symmetric Mode (superscript S). The solid line represents values for the decay case, the broken line the case $y_w=\pm 2375$ km., and the dashed line the case $y_w=\pm 1125$ km.

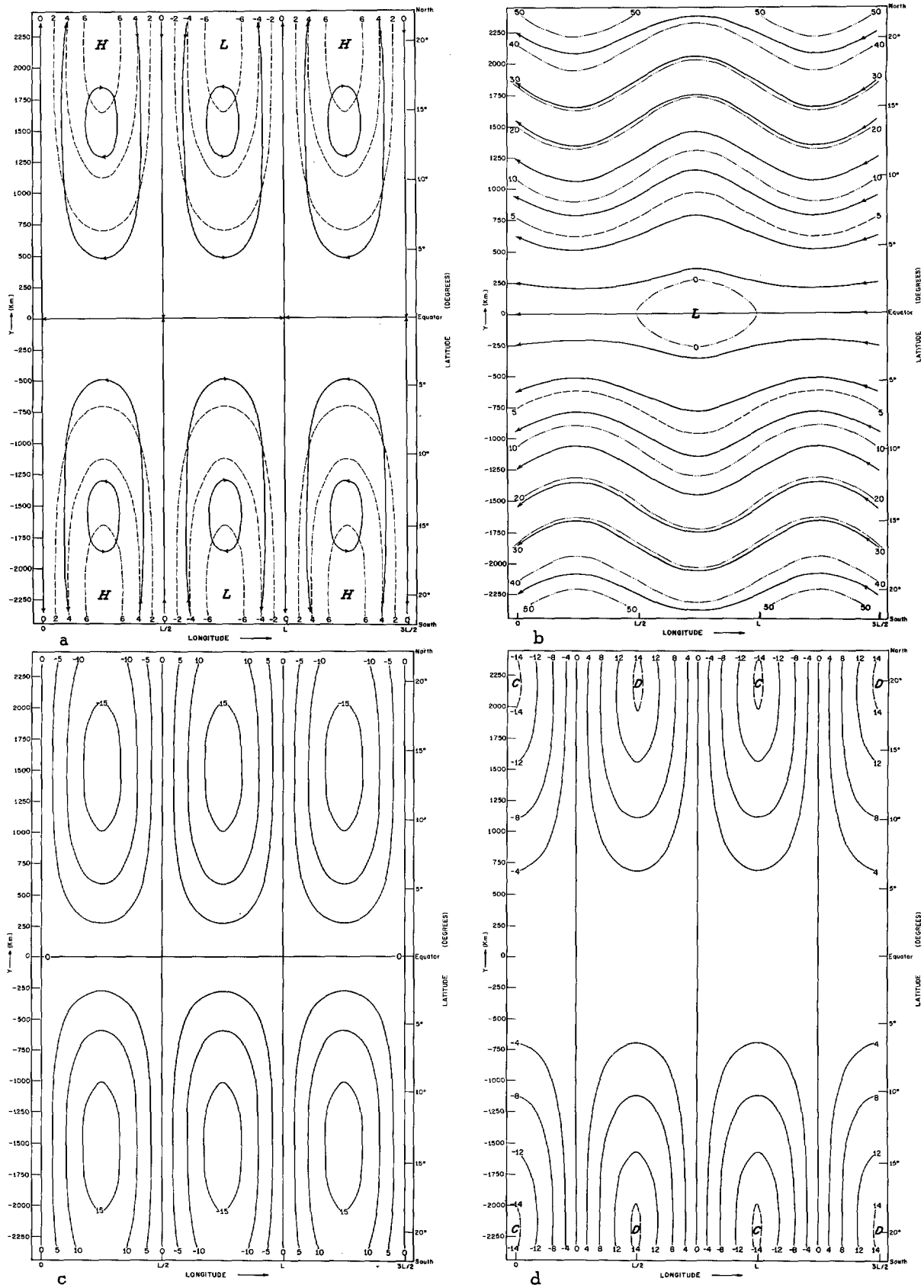

FIGURE 4.—Asymmetric Decay case. (a) Perturbation pressure-height contours (dashed lines) and streamlines (solid lines). Heights are in meters. $v_{max}=5$ m. sec.$^{-1}$, $n=1$, $L=2000$ km., $\sigma=3$ m.t.s. units, $p=1000$ mb., $t=0$. (b) Combined base state and perturbation pressure-height contours (dashed lines) and streamlines (solid lines). Heights are in meters. $U=-7.5$ m. sec.$^{-1}$ Parameters as in (a). (c) Model relative vorticity. Isopleths are labeled in units of 10^{-6} sec.$^{-1}$ Counterclockwise rotation is indicated by positive values. Parameters as in (a). (d) Model divergence. Isopleths are labeled in units of 10^{-8} sec.$^{-1}$ Parameters as in (a).

with $y_w = \pm 1125$ km. Here $p = 1000$ mb., $t = 0$, $\bar{\sigma} = 3$ m.t.s. units, $L = 2000$ km., $n = 1$, and $v_{max} = 5$ m.sec.$^{-1}$ Similar charts were given by Rosenthal [1] for the Symmetric Decay case (with the same values for the various parameters). The figures given here have essentially the same scales which facilitates comparisons. The streamlines shown were constructed from isogon analyses. The base state pressure height fields were computed from the relation $\partial\bar{\phi}/\partial y = -\beta y U$, $U = -7.5$ m./sec.

THE ASYMMETRIC DECAY CASE

Figure 4a shows the pressure-height field and streamlines for the perturbation motion; both fields are symmetric about the equator. The pressure-height and circulation centers are each equidistant from the equator and alternate with longitude. The Highs and Lows are centered near 20° N. and S.; the circulation centers are near 14° N. and S. In both hemispheres, anticyclonic circulation is associated with high pressure and cyclonic motion with low pressure. The pressure centers are characterized by non-zero components of perturbation velocity. Recalling R^A_{0y} (fig. 3) we note these regions are characterized by a highly ageostrophic perturbation u-component. Similarly the equatorial region, where there are non-zero perturbation pressure-height values, is where v is highly ageostrophic (see fig. 2, R^A_{0x}). The maximum magnitude of the perturbation pressure-height is approximately 7 m., which is twice that of the Symmetric Decay case (see Rosenthal, [1] fig. 2).

The combined perturbation and base state height fields and streamlines are shown in figure 4b. Here we find a weak Low (minimum height of −0.4 m.) centered on the equator with an easterly zonal current passing through the center of the Low. The height gradients in the zone bounded by 10° N.–10° S. are very weak and would probably be undetectable in the present-day synoptic observational network.

The relative vorticity and divergence patterns are shown in figures 4c and 4d. The vorticity pattern is asymmetric about the equator with maximum values located about 14° from the equator. Positive values are associated with counterclockwise motion, hence with cyclonic motion in the Northern Hemisphere and anticyclonic motion in the Southern Hemisphere. The opposite is true for the negative values. Therefore, as in the Symmetric Decay case, cyclonic relative vorticity is always associated with low values of perturbation pressure-height. The divergence pattern is symmetric about the equator with maximum values of convergence and divergence about 20° from the equator. Similar to the Symmetric Mode, the divergence centers are to the west of the cyclonic relative vorticity centers and the convergence centers are to the west of the anticyclonic relative vorticity centers. These distributions agree with those previously deduced from the behavior of the wave speed $c = U - \Delta$.

In contrast with the Symmetric Decay case, the total pressure-height field and streamlines (fig. 4b) depict wave disturbances which have maximum amplitude between 10° and 15° from the equator.

THE SYMMETRIC CASE $y_w = \pm 1125$ KM.

The configuration of pressure patterns and streamlines for this case are similar to those of the decay case discussed by Rosenthal [1] except that here we note the effect of the vanishing of the perturbation meridional wind component at a finite distance from the equator. Figure 5a shows the perturbation pressure-height field and streamlines. As in the decay case, the height field is asymmetric about the equator and consists of alternating Highs and Lows. The maximum amplitude is slightly larger than 1 m. which is about one-third that of the decay case. The circulation centers are alternating clockwise, counterclockwise cells centered on the equator and, of course, the perturbation circulation reduces to east-west motion at $y_w = \pm 1125$ km.

The combined perturbation and base state pressure-height field and streamlines are depicted in figure 5b. The streamline pattern is essentially that of the decay case except that the amplitude of the streamlines vanishes near 10° N. and 10° S. At these latitudes the ageostrophic character of the wind field is shown by the fact that the streamlines and pressure-height contours are out of phase. The minimum pressure-heights in the equatorial Lows are approximately −0.2 m.

The relative vorticity pattern (fig. 5c) consists of alternating positive and negative centers which coincide with the perturbation circulation centers (fig. 5a). Low (high) perturbation pressure-height values are coupled with cyclonic (anticyclonic) motion. The configuration of the divergence pattern (fig. 5d) is also similar to the decay case with divergence (convergence) to the west of the cyclonic (anticyclonic) relative vorticity. In comparison to the decay case, we find (1) a reduction of the amplitude of the pressure-height perturbation, (2) marked decreases in the amplitude of the model divergence, and (3) a slight increase in the amplitude of the model relative vorticity.

THE ASYMMETRIC CASE $y_w = \pm 1125$ KM.

The remarks concerning the symmetry and relative distributions of the various fields presented in the discussion of the Asymmetric Decay case apply also to this case. Here we will note the differences in the distributions. Figure 6a shows the pressure-height contours and streamlines of the perturbation motion. The circulation and pressure centers are nearly coincident but the amplitude of the pressure-height field is less than that in the decay case. The combined base state and perturbation height field and streamlines (fig. 6b) have the same character as those in the decay case except the Low centered on the equator has a slight increase in amplitude (to −0.6 m.).

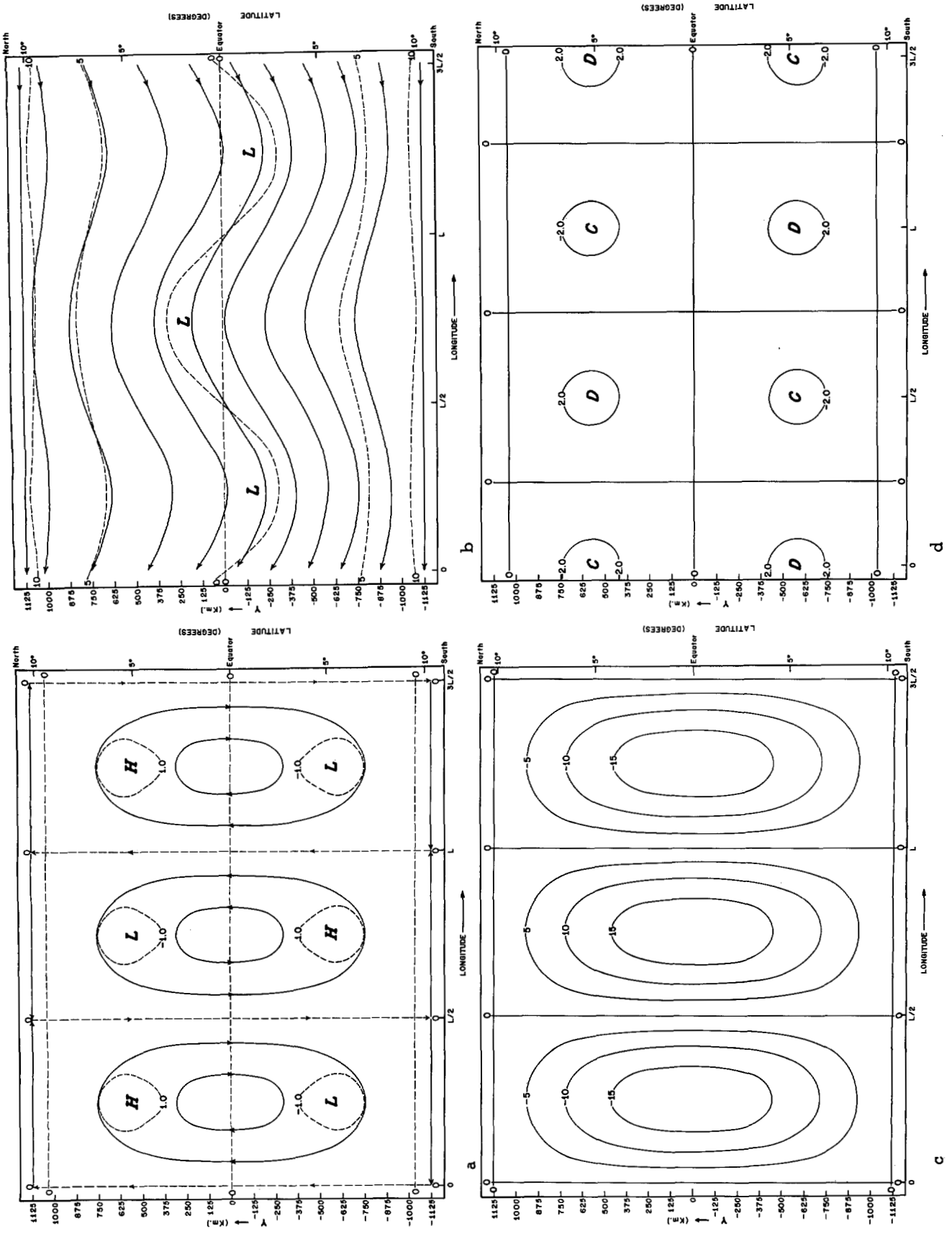

FIGURE 5.—Symmetric case $y_w = \pm 1125$ km. (a) Perturbation pressure-height contours (dashed lines) and streamlines (solid lines). (Coincident height contours and streamlines are dashed). Heights are in meters. Parameters as for figure 4a. (b) Combined base state and perturbation pressure-height contours (dashed lines) and streamlines (solid lines). Heights are in meters. $U = -7.5$ m. sec.$^{-1}$ Parameters as for figure 4a. (c) Model relative vorticity. Isopleths are labeled in units of 10^{-6} sec.$^{-1}$ Counterclockwise rotation is indicated by positive values. Parameters as for figure 4a. (d) Model divergence. Isopleths are labeled in units of 10^{-8} sec.$^{-1}$ Parameters as for figure 4a.

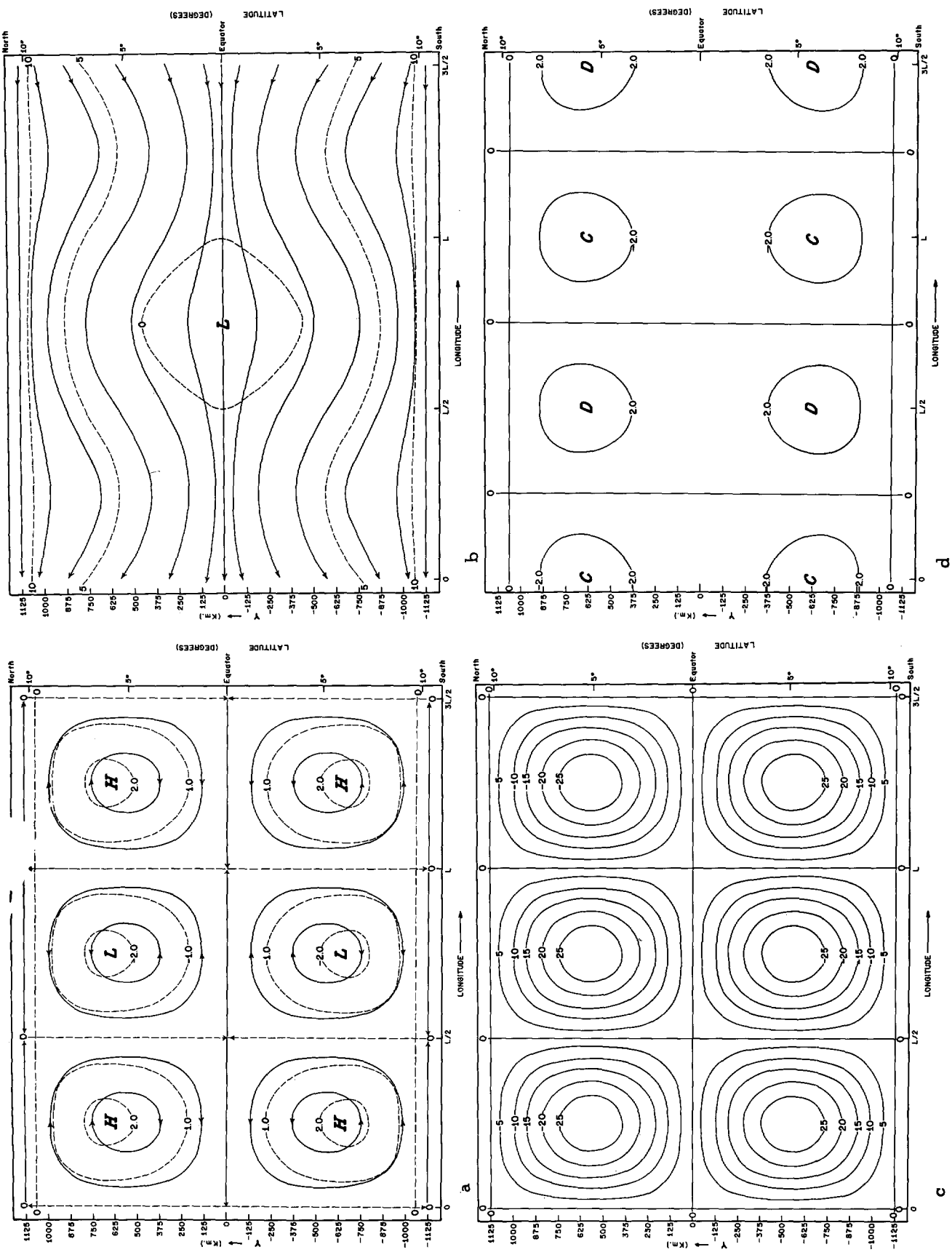

FIGURE 6.—Asymmetric case $y_w = \pm 1125$ km. (a) Perturbation pressure-height contours (dashed lines) and streamlines (solid lines). (Coincident height contours and streamlines are dashed). Heights are in meters. Parameters as for figure 4a. (b) Combined base state and perturbation pressure-height contours (dashed lines) and streamlines (solid lines). Heights are in meters. $U = -7.5$ m. sec.$^{-1}$ Parameters as for figure 4a. (c) Model relative vorticity. Isopleths are labeled in units of 10^{-6} sec.$^{-1}$ Counterclockwise rotation is indicated by positive values. Parameters as for figure 4a. (d) Model divergence. Isopleths are labled in units of 10^{-6} sec.$^{-1}$ Parameters as for figure 4a.

The relative vorticity and divergence patterns are shown in figures 6c and 6d. In this mode, the effects of decreasing the lateral extent of the disturbance are similar to those in the Symmetric Mode except for a slight increase in the amplitude of the equatorial Low in the total pressure-height field.

5. SUMMARY AND CONCLUSIONS

We have considered adiabatic, inviscid, quasi-hydrostatic, β-plane motions in which the perturbation meridional velocity component v is (A) symmetrically, and (B) asymmetrically distributed about the equator. The base state flow was taken as a constant easterly current. In these two modes of motion, v was constrained to vanish (1) as the distance from the equator approached infinity, and (2) at selected finite distances from the equator. Under these conditions, the solutions yield distributions and magnitudes of pressure-height and relative vorticity which are reasonable and meteorologically acceptable. The magnitude of the model divergence is, however, considerably smaller than observed values [3]. This is the result of the adiabatic, nonviscous constraints placed upon the motions. The magnitude of the model pressure-height gradient is extremely small; for this reason the perturbations studied here would probably be undetectable in the pressure field with present observational systems.

The wave speeds for all cases considered are such that the waves progress westward faster than the basic current, but less rapidly than the analogous nondivergent waves. The departures from the nondivergent wave speeds are considerable at longer wavelengths, especially in the Asymmetric Mode. Hence, in all cases, the divergence pattern is such that the westward movement of the perturbation is retarded; there is divergence (convergence) to the west of cyclonic (anticyclonic) relative vorticity. In both modes, the model divergence increases with the perturbation wavelength except in the Symmetric Mode when the meridional extent of the perturbation is small. Equatorial waves of small meridional extent have maximum divergence for mid-range values of wavelength, and become less divergent with increases in wavelength. Also, in both modes, the motions become less divergent as the meridional extent of the perturbation is decreased.

The model relative vorticity decreases with wavelength except in the Asymmetric Mode when the meridional extent of the wave is small. Here the relative vorticity increases at longer wavelengths because of the dominating role of the meridional shear of the zonal component of perturbation wind.

Perturbations centered on the equator have north-south components of velocity which (1) are near geostrophic at low latitudes, (2)become less geostrophic as the meridional extent of the disturbance is decreased, and (3) become less geostrophic as the perturbation wavelength is increased. Perturbations which are centered off the equator have meridional velocity components which are near geostrophic only in the latitudinal zones associated with their circulation centers. In both modes, the east-west velocity component is near geostrophic only at large distances from the equator. In the above remarks, "near" geostrophic implies that the ratios R_{0x}, R_{0y} are approximately 0.2 or less. This condition holds for only certain values of the parameters, and then it may hold over only a part of the latitudinal zone being considered. In general, the acceleration terms are at least the same order of magnitude as the Coriolis term and, hence, their role in the wind-pressure balance cannot be ignored

In a series of numerical experiments conducted at the National Hurricane Research Laboratory, the symmetric solutions (equations (21)–(24), (26)–(29)) to the linearized equations (1)–(4) were used as initial and boundary conditions for a numerical non-linear primitive equation forecast model. In the cases considered, the patterns moved with very nearly the wave speeds deduced above and with very little distortion over four days of real time. This indicates that for the types of motion considered here, the solutions to the linear equations are extremely good approximations to the non-linear solutions.

APPENDIX

Equation (13) can be written as

$$\Delta(\Delta+\gamma)(\Delta-\gamma)+\frac{\gamma\beta}{k^2}[\gamma-(2\alpha+1)\Delta]=0 \qquad \text{(A1)}$$

which is factorable when $\alpha=0$.

For non-zero values of α the roots are

$$\Delta_3=[\sqrt{A^3+B^2}-B]^{1/3}-[\sqrt{A^3+B^2}+B]^{1/3} \qquad \text{(A2)}$$

$$\Delta_2=-\frac{\Delta_3}{2}+\sqrt{-3\left(\frac{\Delta_3^2}{4}+A\right)} \qquad \text{(A3)}$$

and

$$\Delta_1=-\frac{\Delta_3}{2}-\sqrt{-3\left(\frac{\Delta_3^2}{4}+A\right)} \qquad \text{(A4)}$$

where

$$A=-\left[\gamma^2+(2\alpha+1)\cdot\frac{\gamma\beta}{k^2}\right]/3$$

and

$$B=\frac{\gamma^2\beta}{2k^2}.$$

ACKNOWLEDGMENTS

Dr. Stanley L. Rosenthal critically reviewed the manuscript and made suggestions which contributed to its final form. Mr. Robert L. Carrodus drafted the figures, and Miss Deborah Nejman typed the manuscript.

REFERENCES

1. S. L. Rosenthal, "Some Preliminary Theoretical Considerations of Tropospheric Wave Motions in Equatorial Latitudes," *Monthly Weather Review*, vol. 93, No. 10, Oct. 1965, pp. 605–612.
2. T. Matsuno, "Quasi-Geostrophic Motions in the Equatorial Area," *Journal of the Meteorological Society of Japan*, vol. 44, No. 1, Feb. 1966, pp. 25–42.
3. C. E. Palmer, "Tropical Meteorology," *Quarterly Journal of the Royal Meteorological Society*, vol. 78, No. 336, Apr. 1952, pp. 126–164.
4. M. Abramowitz and I. A. Stegun (eds.), *Handbook of Mathematical Functions*, National Bureau of Standards, Washington, D.C., 1964, 1046 pp.
5. J. V. Uspensky, *Theory of Equations*, McGraw-Hill Book Co., Inc., New York, 1948, 353 pp.

[Received February 9, 1967]